Drug Design, Development and Therapy

Dovepress
open access to scientific and medical research

Open Access Full Text Article

ORIGINAL RESEARCH

Extending the application of a magnetic PEG three-part drug release device on a graphene substrate for the removal of Gram-positive and Gram-negative bacteria and cancerous and pathologic cells

This article was published in the following Dove Medical Press journal:
Drug Design, Development and Therapy

M Ramezani Farani[1]
P Khadive Parsi[1]
Gh Riazi[2]
M Shafiee Ardestani[3]
H Saligeh Rad[4,5]

[1]School of Chemical Engineering, University College of Engineering, University of Tehran, Tehran 4563-11155, Iran; [2]Institute of Biophysics and Biochemistry, University of Tehran, Tehran 1417614411, Iran; [3]Department of Radiopharmacy, Faculty of Pharmacy, Tehran University of Medical Sciences, Tehran, Iran; [4]Quantitative Medical Imaging Systems Group, Research Center for Molecular and Cellular Imaging, Tehran University of Medical Sciences, Tehran, Iran; [5]Medical Physics and Biomedical Engineering Department, Tehran University of Medical Sciences, Tehran, Iran

Objective: In this study, novel graphene oxide (GO)-based nanocomposites are presented. In fact, we have tried to replace the carboxyl groups on the surface of GO with amine groups to allow the biocompatible poly(ethylene glycol) bis(carboxymethyl) ether (average Mn 600) polymer to bond through an amide bond.

Materials and methods: The synthesis was conducted accurately according to final characterization experiments (Raman, X-ray diffraction [XRD], atomic force microscopy [AFM], X-ray photoelectron spectroscopy [XPS], thermogravimetric analysis [TGA], etc). The antimicrobial property of this nanocomposite was examined in *Escherichia coli* (ATCC 25922) as Gram-negative and *Staphylococcus aureus* (ATCC 25923) as Gram-positive bacterial species. Besides, curcumin (CUR) was added to the produced nanocomposite both as a promising anticancer drug and an antioxidant, the toxicity of which was then assessed on cellular-based HepG2 and pC12.

Results: An intense increase in toxicity was detected by MTT assay.

Conclusion: It can mainly be concluded that the nanocomposite synthesized in this study is capable of delivering drugs with antibacterial properties.

Keywords: graphene oxide, magnetic nanocomposite, drug delivery, antimicrobial, curcumin

Plain language summary

The nanocarrier G-NH_2–iron oxide nanoparticle (IONP) was prepared as an antibacterial agent. Biocompatible poly(ethylene glycol) (PEG) bis(carboxymethyl) ether (average Mn 600) was bonded through the formation of amide bonds to the substrate. Curcumin (CUR) was loaded onto the G-NH_2–IONP–PEG by π–π stacking interactions. The G-NH_2–IONP–PEG nanocomposite presented a marked antibacterial property.

Introduction

Currently, nanotechnology, a kind of multipurpose scientific technology is used for the fabrication of molecular scale-operating systems or devices, which has resulted in remarkable alterations in different scientific areas.[1] The growth and flourishment of nanotechnology in different scientific fields provide the basis for application of main engineering principles and manipulation at the molecular level.[2] A transition system far smaller than the identifiable target is required for accurate and effective drug

Correspondence: P Khadive Parsi
School of Chemical Engineering, University College of Engineering, University of Tehran, Tehran 4563-11155, Iran
Email kparsi@ut.ac.ir

M Shafiee Ardestani
Department of Radiopharmacy and Medicinal Chemistry, Faculty of Pharmacy, Tehran University of Medical Sciences, Tehran 1417614411, Iran
Email shafieeardestani@sina.tums.ac.ir

submit your manuscript | www.dovepress.com
Dovepress
http://dx.doi.org/10.2147/DDDT.S181090

delivery to highly specific targets.[3,4] Considerable attempts have been recently made for the development of nanotechnology application in the formulation of drugs.[5,6] Due to a direct relationship between drug delivery effectiveness and the size of nanoparticles, nanoparticle preparations can provide biological systems with increased drug availability, advancing controlled drug release with persistent therapy courses. Moreover, intracellular drug delivery has become possible by such systems.[7,8] With a diameter of below 1 μm, nanoparticles can be regarded as colloidal systems. Such a tiny scale renders transporter nanoparticles to infiltrate the blood–brain barrier,[9] the pathways of the pulmonary system,[10] the tight ligaments of the blood vessels,[11] and the epithelial cells of the vein and skin[12,13] and affect targeted tissues.[14–16] In addition to dosage reduction, these carriers are also cost-effective.[17] Nanoparticles come with an additional essential advantage in treatment applications which is that the immune system cannot recognize therapeutic agents incorporated into nanoparticles, and hence, do not stimulate an immune system reaction.[18,19]

Bonded by the Sp^2 hybrid bonds, graphene consists of two-dimensional (2D) sheets of carbon atoms with a hexagonal conformation (honeycomb).[3] Graphene is a state-of-the-art material in the multidimensional graphite carbon family, which includes fullerene as a zero-dimensional (0D) nanomaterial, carbon nanotubes as a one-dimensional (1D) nanomaterial, and graphite as a three-dimensional (3D) material.[20,21] The main structure of graphene breakdowns due to the existing oxygen groups, which render it without good graphene features, including conductivity (electrical–thermal). However, the presence of oxygen groups enables better interaction of graphene with other substances, allowing the attachment of these plates to polymers or covalent bond materials.[22] In addition, it presents a superior biocompatibility and has potential uses in medical industry,[14] fabrication of lightweight composites,[23] nanocarrier in medicine,[24] and in biosensors.[25] Given the use of graphene oxide (GO) as a nanocarrier in drug delivery systems, polymeric coatings, eg, polyethylene glycol (PEG) or dextran (DEX), they are being developed aiming at boosting the efficiency and control of GO function in biological environments, which is apparently absent in dosage toxic tests.[26]

As an ether compound, PEG has various industrial and medical applications.[27] The general formula of PEG is H(OCH2CH2)nOH, with condensed ethylene oxide polymers and water, and it is considered as the most important commercial type of polyether group.[26] It is the first polymer approved by Food and Drug Administration (FDA) for its most important characteristics.[28] There are various applications for PEGs with different molecular weights and varying physical properties, although they have almost similar chemical properties.[21] PEG dissolves in water, methanol, gasoline, and dichloromethane but not in hexane and ethylene ether.[29] Adsorption of proteins through hydrophilic surfaces is impossible, so these molecules adhere to the surface and grow there, resulting in protein denaturation. PEG has a highly useful application as it allows covalent bonding of proteins and drugs by increasing the half-life of drugs.[11]

The effectiveness of electrostatic loading of antacids and insoluble anticancer drugs on GO has also been evaluated in numerous investigations.[30] Curcumin (CUR) or diferuloylmethane is an active ingredient of turmeric shown to have anti-inflammatory properties.[31] As a potent antioxidant, CUR comes with vast therapeutic features.[32] Reports indicate that anticancer substances such as CUR and compote (CPT) holding aromatic rings are loadable on graphene resulting in a high performance.[26,32]

In this study, we synthesized the nanocomposite G-NH_2–iron oxide nanoparticle (IONP)–PEG first. In fact, amine groups first replaced carboxyl-related OH groups present on the surfaces of GO manufactured with a modification of the Hummer method. Furthermore, the abovementioned surfaces were also coated with superparamagnetic nanoparticles (Fe_3O_4) hydrothermally. After that, polythene glycol decarboxylate as a biocompatible polymer formed a covalent bond with the nanocomposite. Finally, the effects of this nanocomposite on the physicochemical, biological, antimicrobial, and drug delivery properties are presented and discussed.

Materials and methods

Materials

Graphite powder, ethanol, iron (III) chloride hexahydrate 98% ($FeCl_3 \cdot 6H_2O$), *N*-(3-dimethylaminopropyl-*N*′-ethylcarbodiimide) hydrochloride (EDC), *N*-hydroxysuccinimide (NHS), sodium acrylate (CH2=CHCOONa), sodium acetate (NaOAc), ethylene glycol (EG), triethylamine (TEA), diethylene glycol (DEG), thionyl chloride ≥99% ($SOCl_2$), dimethylformamide (DMF), methylene chloride (CH_2Cl_2), sodium azide (NaN_3), hydrochloric acid (HCl), poly(ethylene glycol) bis(carboxymethyl) ether (average Mn 600) (PEG), sodium nitrate ($NaNO_3$), hydrogen peroxide (H_2O_2), sulfuric acid, acetone, citric acid, and potassium permanganate were procured from Sigma-Aldrich Co. (St Louis, MO, USA). CUR was purchased from Pakhsh Razi Co., Ltd (Tehran, Iran).

Methods

Synthesis of G-NH_2–IONP–PEG

As defined previously, GO was formulated by a modification of Hummer's method.[1] Concisely, graphite (0.5 g) plus sodium nitrate (0.5 g) were stirred in an ice bath at 300 rpm. Sulfuric acid 98% (23 mL) was then added to the mixture and left stable for 4 hours, followed by the addition of $KMnO_4$ (3 g) to the solution with an increased temperature of 35°C within 1 hour. The resultant biphasic solution comprised water and a golden powder in the upper and lower phases, respectively. Thereafter, H_2O_2 was poured into the solution and ultrasonicated for half an hour. The final solution was washed with distilled water, centrifuged repeatedly until pH rose to ~7, and the precipitate dried at room temperature. In order for the amine groups to replace the carboxyl OH group, dried GO (1 g) was dissipated in 60 mL of thionyl chloride ($SOCl_2$) for 2 hours. DMF (3 mL) was then added to the gas under conditions of N_2 gas injection at 70°C within 24 hours. Next, DMF (120 mL), trimethylamine (10.1 g), ammonia solution (5 g), and distilled water were added to the reaction solution and left at 0°C for 1 hour.

The final solution was filtered using a 0.22 µm filter and then dried.[17,34] To confirm the replacement with the amine group, the Kaiser assay test was done, and the color change of the Kaiser solution to blue showed that this process was done correctly.

In the following step, G-NH_2 (20 mg), $FeCl_3 \cdot 6H_2O$ (270 mg), sodium acrylate (750 mg), and sodium acetate (750 mg) were dissolved in a mixture of EG (0.5 mL) and DEG (9.5 mL). The final solution was then transferred to a Teflon-lined stainless steel autoclave and incubated in an oven at 200°C for 12 hours. The obtained solution (G-NH_2–IONP) was rinsed frequently with deionized water and ethanol solution and dried in vacuum for 15 hours.[12,14] Afterward, enough ammonium 25% solution was added to elevate the pH of solution to 8, and then 100 µL of PEG bis(carboxymethyl) ether (600 Da) was poured into the G-NH_2–IONP solution (25 mL) and sonicated for 15 minutes. This was followed by adding 10 mg of NHS, and 15 minutes later 30 mg of EDC was added to the solution. The reaction vessel was then covered with an aluminum foil and the mixture stirred at ambient temperature overnight. To eliminate unreacted PEG and other reagents, the resultant product (G-NH_2–IONP–PEG) was filtered using a dialysis bag (5 Da) for 24 hours. The final solution was subjected to characterization tests after drying.[28,35]

Preparation of G-NH_2–IONP–PEG–CUR

Parallel to loading CUR, G-NH_2–IONP–PEG (0.01 g) was first fully dissipated in deionized water (20 mL) by an ultrasonic probe at 20°C for 15 minutes. Thereafter, CUR (0.004 g) was dissolved in purified acetone (2 mL), and the prepared solution was slowly dripped into the G-NH_2–IONP–PEG solution. The final mixture was gently spun at normal temperature conditions for roughly 24 hours, and the obtained mixture was rotated around via centrifugation at 4,000 rpm for 15 minutes, followed by effective separation of the pellet and supernatant. Unbound CUR was removed through centrifugation at 3,500 rpm for 15 minutes.[7] A great attempt was made to specify the encapsulation efficiency (EE) and drug loading (DL) capacity of CUR in G-NH_2–IONP–PEG, after which G-NH_2–IONP–PEG–CUR was dispersed in dimethyl sulfoxide (DMSO) (Figure 1).[8]

Finally, the released CUR was accurately quantified by UV-Vis at 420 nm. Using the following Equations 1 and 2, both DL and EE factors were obtained for CUR loaded on G-NH_2–IONP–PEG:

$$\text{EE (\%)} = \frac{\text{Total amount of CUR} - \text{Free CUR in percipitate}}{\text{Total amount of CUR}} \times 100 \quad (1)$$

$$\text{DL (\%)} = \frac{\text{Total amount of CUR} - \text{Free CUR in percipitate}}{\text{Mass of final formulation}} \times 100 \quad (2)$$

CUR release assay

In vitro examinations on drug release were conducted at pH values of 7.4 and 5 in a normal environment for 48 hours at intervals. G-NH_2–IONP–PEG–CUR (10 mg) was added to citrate buffer (pH 5) or 20 mL of PBS (pH 7.4), and the final product was mildly stirred in a shaker incubator at 60 rpm and a temperature of 37°C for 5, 20, 24, and 48 hours. To precipitate water-insoluble CUR, each formulation was centrifuged at 1,500 rpm for 5 minutes, the supernatant of which contained the loaded CUR on the G-NH_2–IONP–PEG surface. The precipitate was dissolved in DMSO (1 mL), and the released CUR was quantified using UV-Vis at 420 nm.[32,36]

Cellular viability assay

In a normal RPMI 1640 culture medium containing 10% FBS and penicillin (100 U/mL)/streptomycin (100 µg/mL), murine hepatocellular carcinoma cells (HepG2 cell lines),

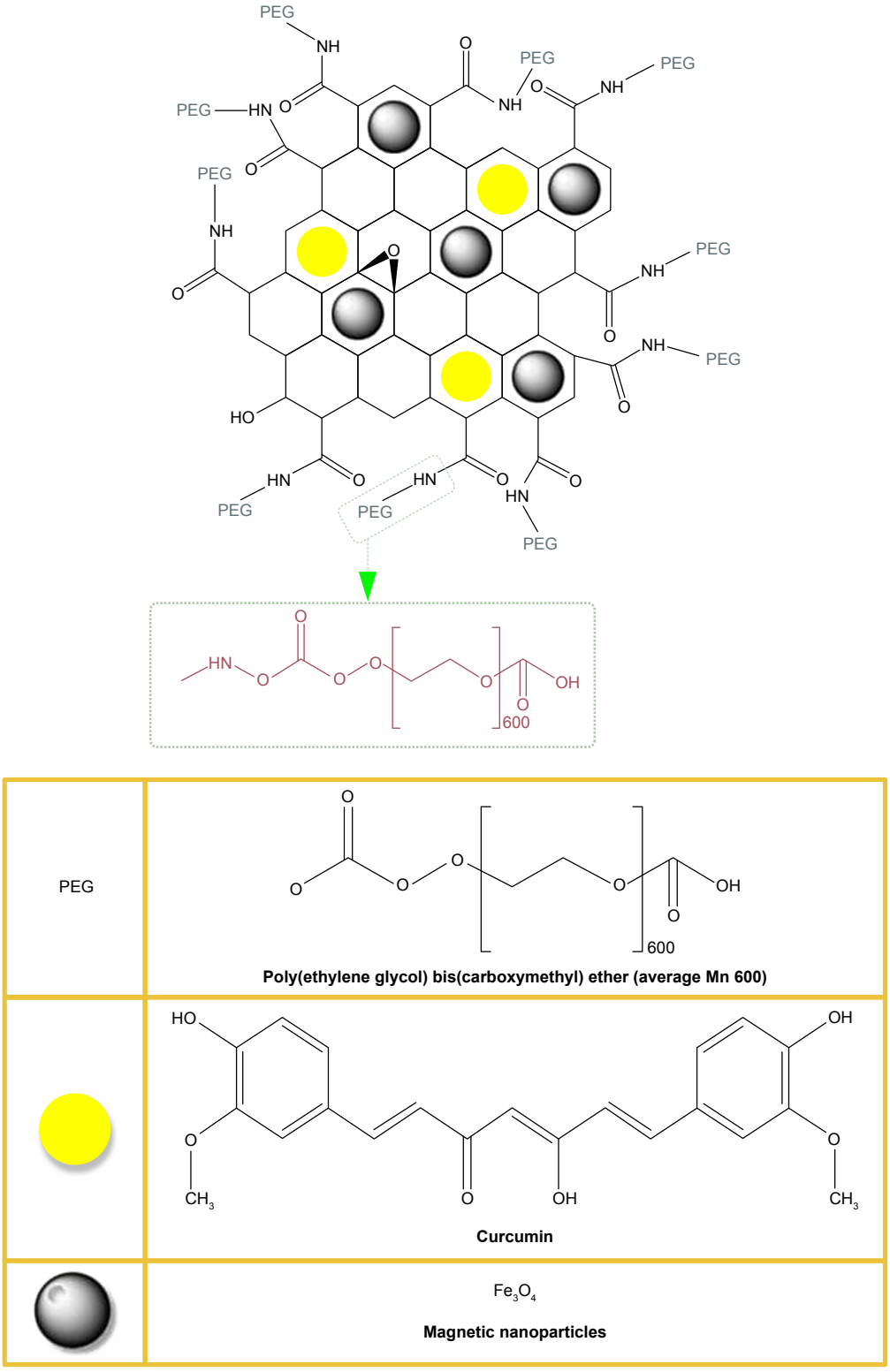

Figure 1 A schematic view of G-NH_2–IONP–PEG synthesis.
Abbreviation: IONP, iron oxide nanoparticle.

purchased from Pasteur Institute of Iran, were added at 37°C and 5% CO_2. The cells with a density of 5×10^4 cells/well were poured into a 96-well tissue culture plate. The subsequent day, the same amounts (up to 300 µg/mL) of free CUR and G-NH_2–IONP–PEG–CUR were used to treat cells in a complete medium (100 µL) with 10% FBS during 6 hours. Following removal of the medium, the cells were washed with PBS, exposed to RPMI (100 µL) with 10%

FBS, and incubated again at 37°C for 24 and 48 hours.[32] Ten microliters of 5 mg/mL MTT in PBS were poured to each well and incubated for 4 hours. Formazan crystals were dissolved in 150 µL of DMSO, and the absorbance was assessed at 570 nm wavelength using an ELISA reader,[37] which was repeated for PCL2 cells.[14,38]

The reported observations were obtained from a Carry 100 Bio (Varian) microprobe at a wavelength of 590 nm, with 630 nm as the reference wavelength.

Antimicrobial assay

Through the antibacterial drop test, the bactericidal activities of all the samples toward *Escherichia coli* (ATCC 25922) and *Staphylococcus aureus* (ATCC 25923) as Gram-negative and Gram-positive bacteria, respectively, were examined.[39] The bacteria were freshly cultured in a nutrient agar plate at 37°C for 24 hours for use in microbiological assays. The cultured bacteria were added to a saline solution (10 mL) to increase bacterial density, resulting in the formation of 10^8 colony-forming units per milliliter (CFU/mL). Individual samples were sterilized in separate Petri dishes, then the diluted bacterial suspension (100 L), already diluted to 10^6 CFU/mL, was added on each sample. The samples were finally centrifuged at 37°C for 60 minutes followed by the removal of the bacteria from the supernatant using PBS (5 mL) in a sterile Petri dish.

After establishment of the bacterial suspension (100 L) on an agar plate, it was incubated at 37°C overnight. The remaining bacterial colonies were ultimately counted via optical microscopy.[40,41]

Results and discussion

Structural characterization

The OH-carboxyl groups on the surface were replaced by the amine groups upon synthesis of GO by an altered Hummer's method. The superparamagnetic nanoparticles were then deposited in a codeposited manner. Finally, amide bonds were formed by bonding the polyethylene glycol dicarboxylic polymer through covalent bonds to amine groups (Figure 1).

Figure 2 shows the produced nanocomposite as an atomic force microscopy (AFM) image of a graphite-active oxidation sample. It characterizes magnetite nanoparticles containing amine groups covered with PEG. The distribution

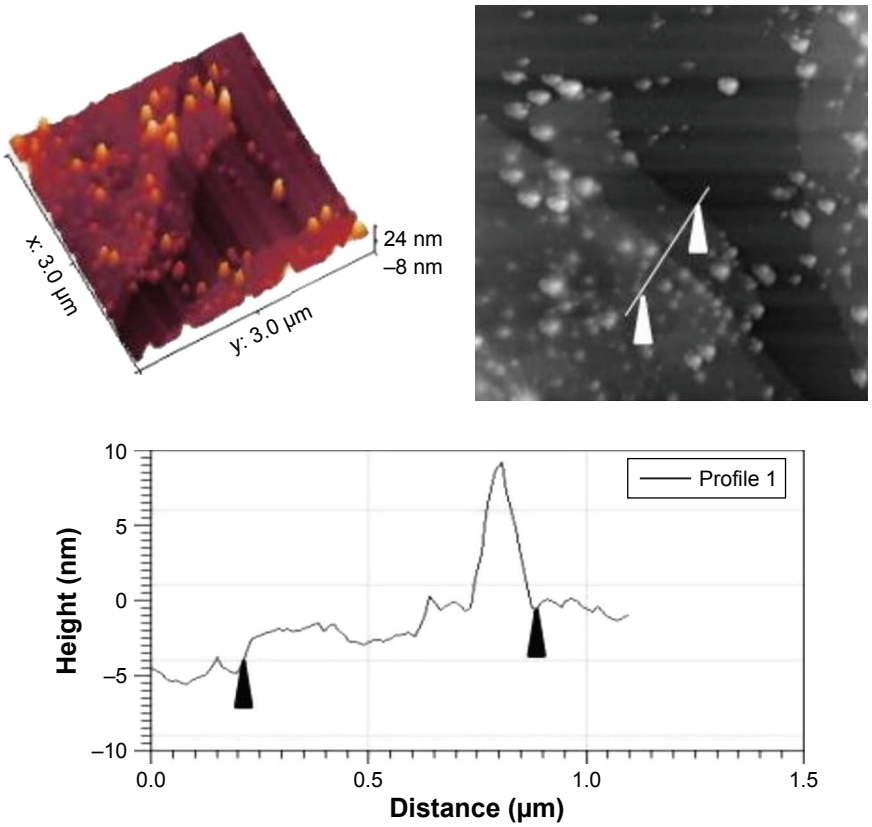

Figure 2 Atomic force microscopy of graphene oxide operated by magnetite nanoparticles containing amine groups coated with polyethylene glycol on the mica surface along with the height distribution chart.
Notes: White arrows indicate the location of desired points for height evaluation.

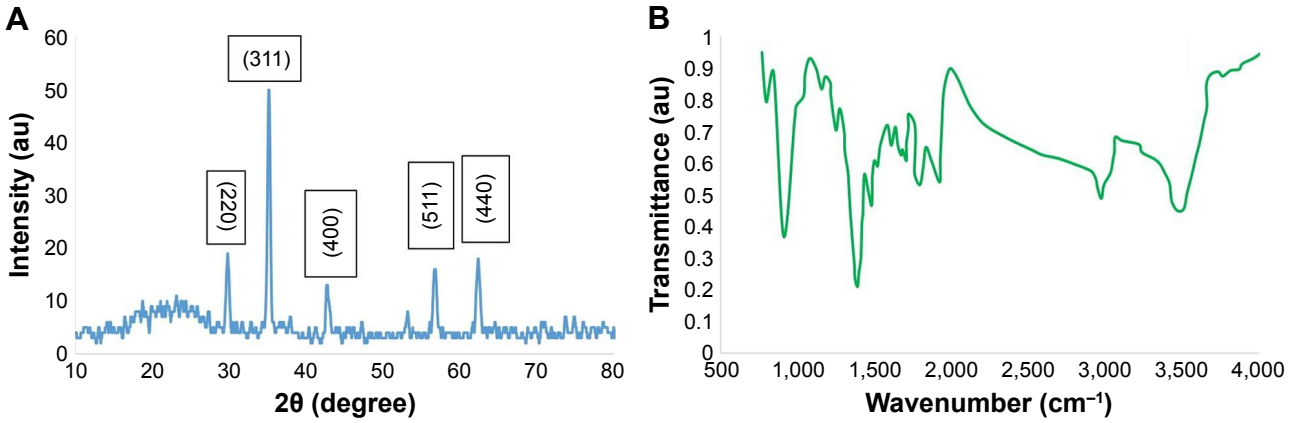

Figure 3 (**A**) X-ray diffraction pattern of G-NH_2–IONP–PEG. (**B**) FTIR spectra of G-NH_2–IONP–PEG.
Abbreviations: FTIR, Fourier-transform infrared spectroscopy; IONP, iron oxide nanoparticle.

of IONPs (average size of 10 nm) is well illustrated, which corresponds to the result of XRD. Clearly, a thickness of 10 nm for magnetite particles and a 1–2 nm difference in surface layer of overlapping GO bilayer are shown in Figure 2.[12] A comparison of the diffraction pattern resulted from the sample and the reference diffraction patterns (Figure 3A) determines the type of iron oxide present in the samples. The diffraction pattern of the iron oxides illustrates various carriers. To compare the reference peaks for Fe_2O_3 or Fe_3O_4, confirm that the a strong (311) peak at $2\theta = 35.5°$. The location of the second and third couriers is (in terms of intensity) in the diffraction patterns of each material in a different location. The second peak is a (400) peak at $2\theta = 43.2°$ and the third (422) peak at $2\theta = 57.2°$, while the location of the hematite is displaced. The type of iron oxide associated with Fe_3O_4 particles can be determined from the reference diffraction patterns through comparison of the diffusion pattern obtained from the synthesized nanoparticles. The described carriers conform to the JCPDS reference No 89-3854 Fe_3O_4 reference correlation, confirming a successful synthesis.[14,18] Fourier-transform infrared spectroscopy (FTIR) spectroscopy was done to investigate the structure of the synthesized nanocomposite. A significant peak in the region of 1,573 cm^{-1}, which is related to the N–H bond, and the peak located within the range of 950–1,250 cm^{-1} for the C–N tensile bond are observed, and the peak in the 2,900 cm^{-1} region and a range of 900–1,400 cm^{-1} are related to the vibrating bonds of C–H and CO, which confirms the bonding of the PEG to the synthetic structure (Figure 3B).

A classical method called X-ray photoelectron spectroscopy (XPS) is employed for the semiquantitative analysis of surface composition. The occurrence of carbon and oxygen on the structure of GO is presented in Figure 4. The pureness of the synthesized GO is reflected by no impurity peaks in the analytical outcomes. The percentage of each

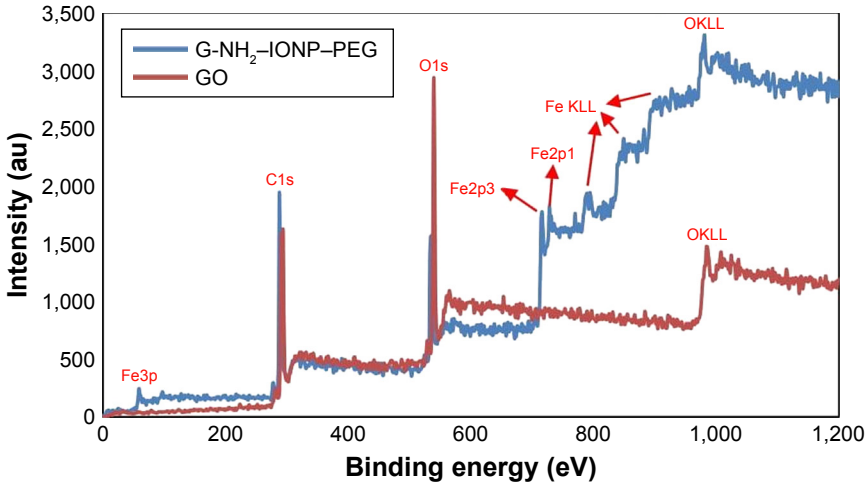

Figure 4 Spectroscopy of X-ray photoelectron of GO and G-NH_2–IONP–PEG.
Abbreviations: GO, graphene oxide; IONP, iron oxide nanoparticle.

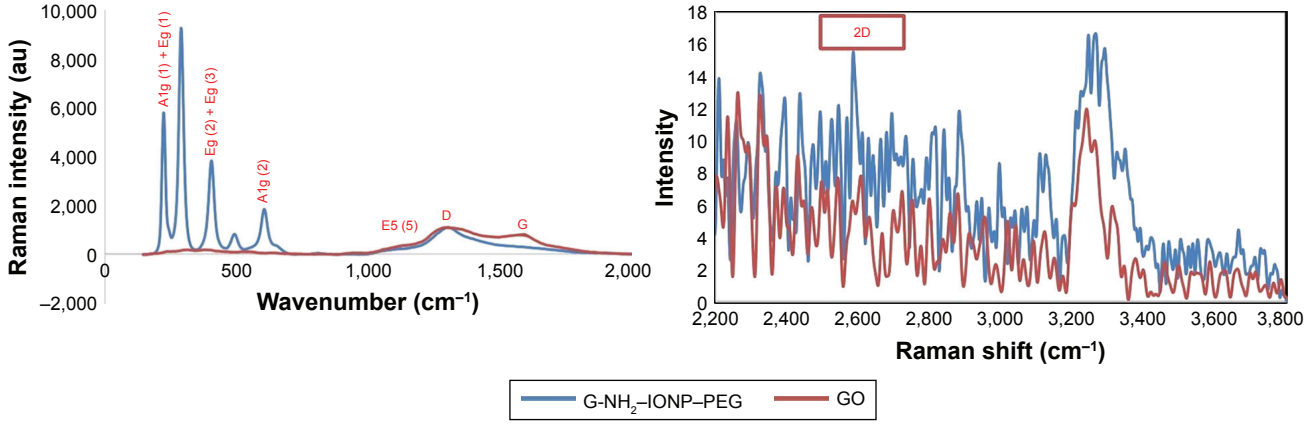

Figure 5 Raman spectrum for magnetite graphene amine samples coated with polyethylene glycol.
Abbreviation: IONP, iron oxide nanoparticle.

atom may be determined as represented by the following peak level assessment yielding 69% and 31% for carbon and oxygen, respectively. These findings are markedly consistent with that of almost 30 for thermal decomposition, including oxygen groups, which also indicates that magnetite is present on GO. Raman spectrum for magnetite graphene amine samples coated with PEG is shown in Figure 5. The magnetized graphene amine sample indicates a considerable reduction in the height ratio of the two peaks D and G, and hence, they are not easily separable leading to the addition of five new peaks, which are representative of the magnetic nanoparticle at 222.5, 289, 404, 492, and 605 cm^{-1} with heights of 5,794.441, 9,264.912, 384.664, and 837.5156, respectively. The number 1,859.133 belongs to the interactions of A1 (g) + Eg (1), Eg (2) + Eg (3), Eg (4), A1g (2) and Eg (5) phonons. A height of 1,119.555 is observed for the magnitude 2D peak appearing at 1,303 cm^{-1}.[14]

Figure 6 illustrates three distinct weight losses in the air environment for thermal gravity gradient decomposition chart (thermogravimetric analysis [TGA]) of GO. At 100°C, the first weight loss of 8% is caused by the evaporation of water between the GO layers. Because the existing oxygen levels (hydroxy, epoxy, and carboxy) comprising ~30% of the weight are removed in the surface, the second weight loss happens in the range of 200°C–250°C. The burning and oxidation of carbon with oxygen in the air at temperatures above 600°C lead to a maximum GO weight loss of nearly 50%. According to these results, it can be estimated that about 30% by weight of GO contains oxygen species groups. In Figure 6, the operating sample of the GO sample with the amine group containing the magnetite nanoparticles

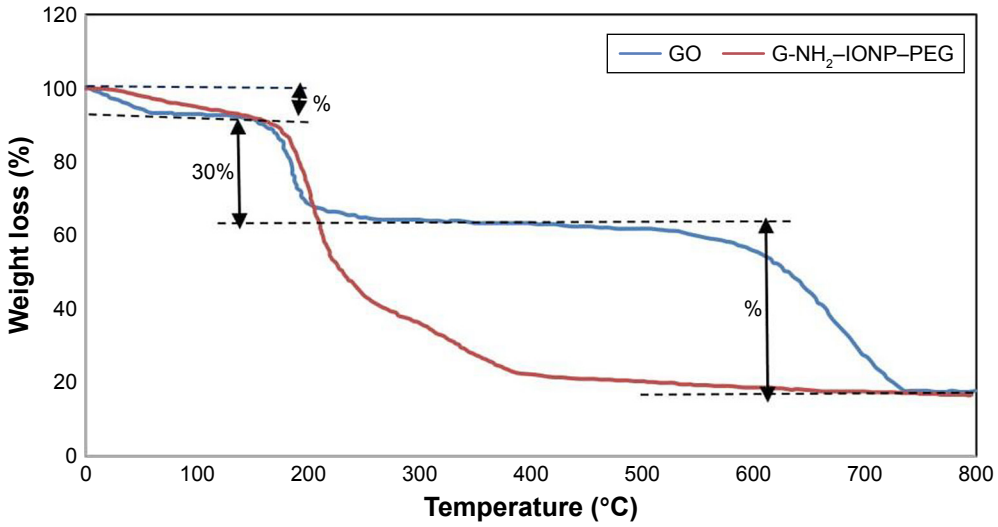

Figure 6 Thermal decomposition diagram of GO and G-NH_2–IONP–PEG.
Abbreviations: GO, graphene oxide; IONP, iron oxide nanoparticle.

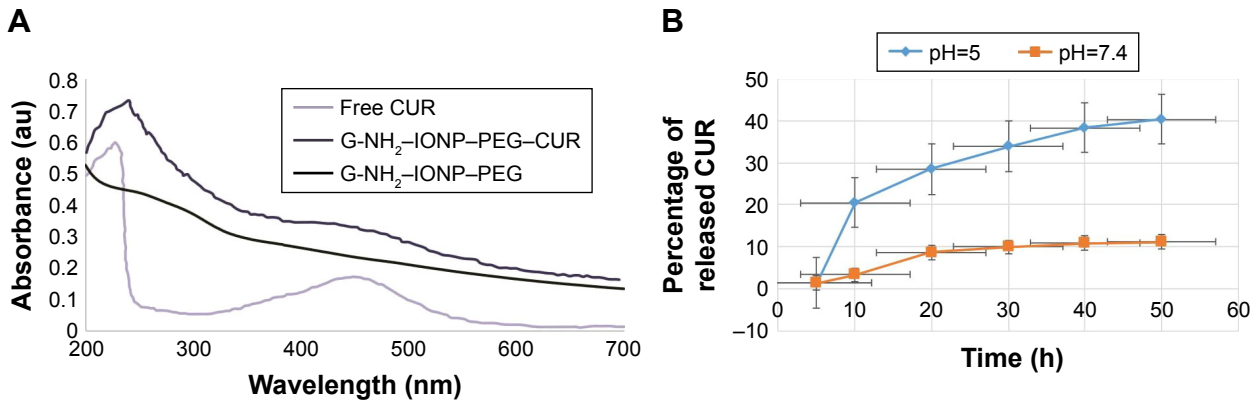

Figure 7 (**A**) UV-visible absorption of G-NH_2–IONP–PEG, G-NH_2–IONP–PEG–CUR, and free CUR. (**B**) Amount of drug-released CUR.
Abbreviations: CUR, curcumin; IONP, iron oxide nanoparticle.

covered with PEG shows that in the range of 100°C–200°C, this weight loss relates to the remaining water in particles. It can be said that the polymer that surrounds the nanoparticle prevents water from escaping. At temperatures ranging from 200°C to 600°C, weight loss occurs at a different rate due to the PEG polymer.[15]

Drug delivery potential

In the form of nanoscale sheet-like system, the G-NH_2–IONP–PEG was evaluated as a carrier of hydrophobic drugs such as CUR. UV-Vis absorbance peak at 420 nm revealed a yellowish solution showing successful loading of CUR on the G-NH_2–IONP–PEG surface. The loading of CUR onto the surface of either G-NH2–IONP–PEG can be attributed to π–π stacking interactions (Figure 7A),[32,36] with calculated EEs of 59.5±12.43 and 70.18±17.78, respectively, based on the equation for CUR loaded on G-NH_2–IONP–PEG. According to the abovementioned equation, DL values of 25.6%±7.35% and 39.22±5.43, respectively, were obtained for CUR loaded on G-NH_2–IONP–PEG. Two different pH values (7.4 and 5) were used to evaluate CUR release from G-NH_2–IONP–PEG sheets, showing a release of ~70% for CUR loaded on both G-NH_2–IONP–PEG over 48 hours in an acidic solution of pH=5 (Figure 7B). However, a release rate of 20%–30% was observed in a neutral solution within the same duration, which is in line with those reported previously.[32]

In vitro cellular cytotoxicity (MTT) assay

The number of viable cells in a given culture was determined by MTT assay. CUR and G-NH_2–IONP–PEG–CUR were also tested at various concentrations (3.12, 6.5, 12.5, 25, and 50 µg/mL) for 48 hours. A very high concentration (50 µg/mL) of G-NH_2–IONP–PEG slightly decreased cell viability. In contrast, results demonstrate that high cytotoxicity at lower concentrations of GO exposure has observed (Figure 8A and B), the *P*-value of whole test is ($P<0.05$) meaning our result in all concentrations significantly decreased. Figure 8A shows cell viability reduction with increase in CUR concentration

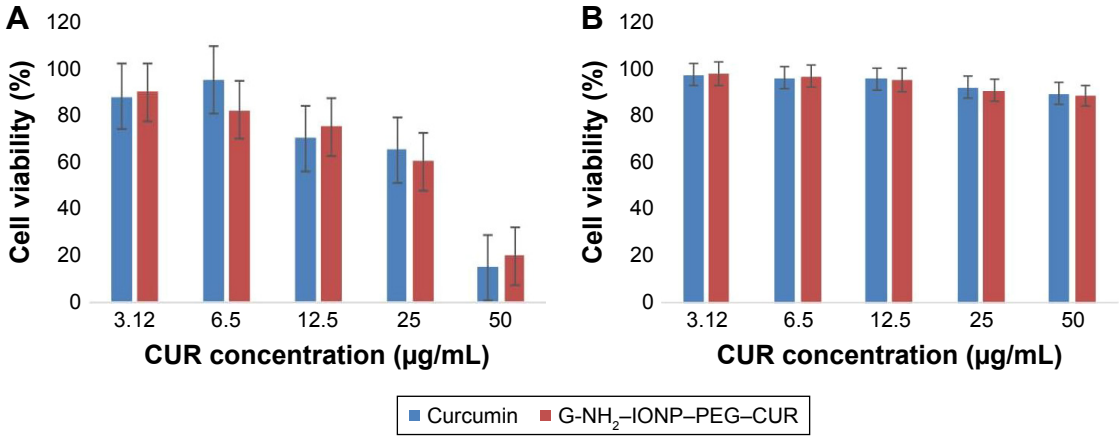

Figure 8 The cytotoxicity of G-NH_2–IONP–PEG–CUR and free CUR (after 48 hours) on: (**A**) HepG2 and (**B**) pC12.
Abbreviations: CUR, curcumin; IONP, iron oxide nanoparticle.

in HepG2 cell line, suggesting that rising concentrations of CUR and G-NH_2–IONP–PEG–CUR will have toxic effects on HepG2 cell line. A significant decrease in HepG2 cell viability was obtained for the whole test ($P<0.05$). For the prepared formulations, the applied carrier concentration was below the toxic level for the cells in all cellular experiments.[32] Our data demonstrate enhanced biocompatibility of PEG conjugation to GO;[42] however, pathological cells presented no changes (Figure 8B). The cellular toxicity of G-NH_2–IONP–PEG–CUR and free CUR was examined and compared by incubation of composites and free CUR with HepG2 cells, giving rise to elevated CUR delivery and cytotoxicity on HepG2 cells.[7] Accordingly, this determines the utmost dosage range for drug transferability by the selective cell killing level.[32,43]

Antibacterial activity

Figure 9 represents the antibacterial activity of nanocomposite against *E. coli* and *S. aureus* by colony counting method. The results of colony counting method (Figure 10) showed that G-NH_2–IONP–PEG inhibited the growth of both bacterial species in a concentration-dependent manner. There are two types of antibacterial activities, namely, bacteriostatic, which prevents the growth of bacteria without killing, and bactericidal which kills the bacteria. Colony counting method confirmed the bactericidal property of GO; it completely inhibited the growth of *E. coli* and *S. aureus* at the concentrations of 100 and 125 µg/mL, respectively.

The observed differential toxicity is due to many factors such as the primary difference between the Gram-negative and Gram-positive bacteria with respect to the nature of their cell wall. In addition to this, the Gram-negative bacteria possess an additional outer membrane comprising lipopolysaccharides that protects the peptidoglycan layer from chemical attacks. It is significant to mention that nanoparticle-mediated toxicity toward bacterial species not only relies on the bacterial structure but also depends on several factors including the enzymatic activity.[44]

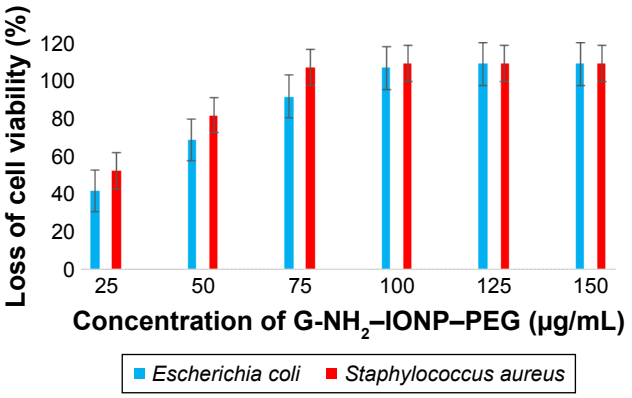

Figure 10 Results of antimicrobial activity of G-NH_2–IONP–PEG by colony counting method.
Abbreviation: IONP, iron oxide nanoparticle.

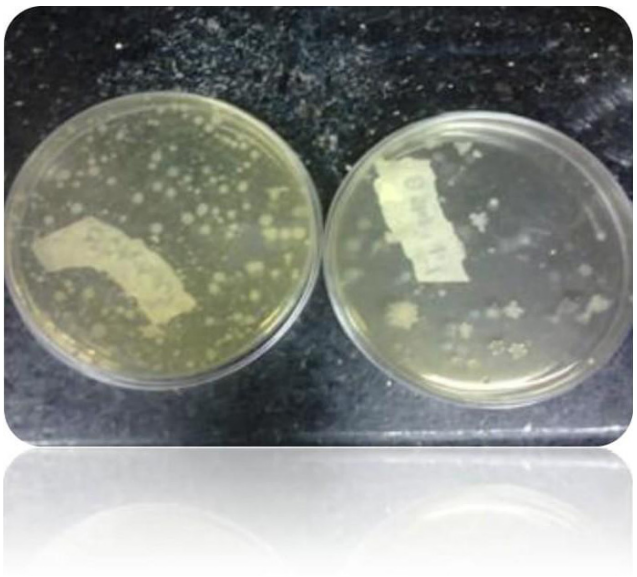

Figure 9 The number of colonies in the control sample immediately after inoculation (right) and 24 hours after inoculation (left).

Conclusion

In this study, an amino-modified GO covered with PEG-coated magnetic nanoparticles were successfully synthesized, which was confirmed by characterization analysis of the nanocomposite. A considerable antibacterial activity of the formulated nanocomposite was established on *E. coli* as a Gram-positive bacterium. Gram-positive bacterium bacteria consist of a relatively thicker peptidoglycan cell wall and thus the carrier cannot pass through into the cytoplasm, rendering a stronger defense system in *S. aureus* than that of *E. coli*. Moreover, a high dose of CUR can be delivered by this nanocomposite depending on the pH, yielding a superior result in acidic conditions.

Disclosure

The authors report no conflicts of interest in this work.

References

1. Kumawat MK, Thakur M, Gurung RB, Srivastava R. Graphene quantum dots from *Mangifera indica*: application in near-infrared bioimaging and intracellular nano-thermometry. *ACS Sustainable Chem Eng*. 2016;6:b01893.
2. Singh SK, Singh MK, Kulkarni PP, Sonkar VK, Grácio JJ, Dash D. Amine-modified graphene: thrombo-protective safer alternative to graphene oxide for biomedical applications. *ACS Nano*. 2012;6(3):2731–2740.
3. Kavita S, Vijayender B, Priyanka S, Roohi K, Shilpa C, Raman S. Amine functionalized graphene oxide/CNT nanocomposite for ultrasensitive electrochemical detection of trinitrotoluene. *Journal of Hazardous Materials*. 2013;248–249:322–328.

4. Ma X, Tao H, Yang K, et al. A functionalized graphene oxide-iron oxide nanocomposite for magnetically targeted drug delivery, photothermal therapy, and magnetic resonance imaging. *Nano Res*. 2012;5(3):199–212.
5. Kim J-H, Lee K-H. Effect of PEG additive on membrane formation by phase inversion. *J Memb Sci*. 1998;138(2):153–163.
6. Mendonça MC, Soares ES, de Jesus MB, et al. PEGylation of reduced graphene oxide induces toxicity in cells of the blood-brain barrier: an *in vitro* and *in vivo* study. *Mol Pharm*. 2016;13(11):3913–3924.
7. Alibolandi M, Mohammadi M, Taghdisi SM, Ramezani M, Abnous K. Fabrication of aptamer decorated dextran coated nano-graphene oxide for targeted drug delivery. *Carbohydr Polym*. 2017;155:218–229.
8. Marković ZM, Kepić DP, Matijašević DM, et al. Ambient light induced antibacterial action of curcumin/graphene nanomesh hybrids. *RSC Adv*. 2017;7(57):36081–36092.
9. Xie B, Yi J, Peng J, et al. Characterization of synergistic anti-tumor effects of doxorubicin and p53 via graphene oxide-polyethyleneimine nanocarriers. *J Mater Sci Technol*. 2017;33(8):807–814.
10. Costantini S, di Bernardo G, Cammarota M, Castello G, Colonna G. Gene expression signature of human HepG2 cell line. *Gene*. 2013;518(2):335–345.
11. Akhavan O, Ghaderi E. Toxicity of graphene and graphene oxide nanowalls against bacteria. *ACS Nano*. 2010;4(10):5731–5736.
12. Ordikhani F, Farani MR, Dehghani M, Tamjid E, Simchi A. Physicochemical and biological properties of electrodeposited graphene oxide/chitosan films with drug-eluting capacity. *Carbon*. 2015;84:91–102.
13. Yuan G, Yuan Y, Xu K, Luo Q. Biocompatible PEGylated Fe_3O_4 nanoparticles as photothermal agents for near-infrared light modulated cancer therapy. *Int J Mol Sci*. 2014;15(10):18776–18788.
14. Yang Y, Asiri AM, Tang Z, Du D, Lin Y. Graphene based materials for biomedical applications. *Materials Today*. 2013;16(10):365–373.
15. Lu Y-J, Wei K-C, Ma C-CM, Yang S-Y, Chen J-P. Dual targeted delivery of doxorubicin to cancer cells using folate-conjugated magnetic multi-walled carbon nanotubes. *Colloids Surfaces B Biointerfaces*. 2012;89:1–9.
16. Kim YK, Kim MH, Min DH. Biocompatible reduced graphene oxide prepared by using dextran as a multifunctional reducing agent. *Chem Commun*. 2011;47(11):3195–3197.
17. Jinzhao L, Jia D, Ting Z, Qiang P. Graphene-based nanomaterials and their potentials in advanced drug delivery and cancer therapy. *Journal of Controlled Release*. 2018;286:64–73.
18. Yuan G, Yuan Y, Xu K, Luo Q. Biocompatible PEGylated Fe_3O_4 nanoparticles as photothermal agents for near-infrared light modulated cancer therapy. *Int J Mol Sci*. 2014;15(10):18776–18788.
19. Ge J, Lan M, Zhou B, et al. A graphene quantum dot photodynamic therapy agent with high singlet oxygen generation. *Nat Commun*. 2014;5:4596.
20. Ozcan F, Ersoz M, Yilmaz M. Preparation and application of calix[4]arene-grafted magnetite nanoparticles for removal of dichromate anions. *Materials Science and Engineering: C*. 2009;29(8):2378–2383.
21. Cole AJ, David AE, Wang J, Galbán CJ, Yang VC. Magnetic brain tumor targeting and biodistribution of long-circulating PEG-modified, cross-linked starch-coated iron oxide nanoparticles. *Biomaterials*. 2011;32(26):6291–6301.
22. Li S, Xiao L, Deng H, Shi X, Cao Q. Remote controlled drug release from multi-functional Fe_3O_4/GO/Chitosan microspheres fabricated by an electrospray method. *Colloids Surf B Biointerfaces*. 2017;151:354–362.
23. Abdullah S, Wendy-Yeo WY, Hosseinkhani H, et al. Gene transfer into the lung by nanoparticle dextran-spermine/plasmid DNA complexes. *J Biomed Biotechnol*. 2010;2010:1–10.
24. Markovic ZM, Harhaji-Trajkovic LM, Todorovic-Markovic BM, et al. In vitro comparison of the photothermal anticancer activity of graphene nanoparticles and carbon nanotubes. *Biomaterials*. 2011;32(4):1121–1129.
25. Hong BJ, Compton OC, An Z, Eryazici I, Nguyen ST. Successful stabilization of graphene oxide in electrolyte solutions: enhancement of bio-functionalization and cellular uptake. *ACS Nano*. 2011;127:1–10.
26. Imani R, Emami SH, Faghihi S. Synthesis and characterization of an octaarginine functionalized graphene oxide nano-carrier for gene delivery applications. *Phys Chem*. 2015;17(9):6328–6339.
27. Angelopoulou A, Voulgari E, Diamanti EK, Gournis D, Avgoustakis K. Graphene oxide stabilized by PLA-PEG copolymers for the controlled delivery of paclitaxel. *Eur J Pharm Biopharm*. 2015;93:18–26.
28. Chu J, Shi P, Yan W, et al. PEGylated graphene oxide-mediated quercetin-modified collagen hybrid scaffold for enhancement of MSCs differentiation potential and diabetic wound healing. *Nanoscale*. 2018;10(20):9547–9560.
29. Özdemir C, Güner A. Solubility profiles of poly(ethylene glycol)/solvent systems, I: qualitative comparison of solubility parameter approaches. *Eur Polym J*. 2007;43(7):3068–3093.
30. Wang G, Shen X, Wang B, Yao J, Park J. Synthesis and characterization of hydrophilic and organophilic graphene nanosheets. *Carbon*. 2009;47(5):1359–1364.
31. Dinesh B, Shalini Devi KS, Kumar AS. Curcumin-quinone immobilised carbon black modified electrode prepared by in-situ electrochemical oxidation of curcumin-phytonutrient for mediated oxidation and flow injection analysis of sulfide. *J Electroanal Chem*. 2017;804:116–127.
32. Kiew SF, Ho YT, Kiew LV, et al. Preparation and characterization of an amylase-triggered dextrin-linked graphene oxide anticancer drug nanocarrier and its vascular permeability. *Int J Pharm*. 2017;534(1–2):297–307.
33. Kumawat MK, Thakur M, Gurung RB, Srivastava R. Graphene quantum dots from mangifera indica: application in near-infrared bioimaging and intracellular nano-thermometry. *ACS Sustain Chem Eng*. 2017;5(2):1382–1391.
34. Huong NT, Giang LTK, Binh NT, Minh LQ. Surface modification of iron oxide nanoparticles and their conjuntion with water soluble polymers for biomedical application. *J Phys Conf Ser*. 2009;187:1–5.
35. Vajihe M, Asghar T, Abdol K. Xylanase immobilization on modified superparamagnetic graphene oxide nanocomposite: Effect of PEGylation on activity and stability. *International Journal of Biological Macromolecule*. 2018;107:418–425.
36. Xie B, Yi J, Peng J, et al. Characterization of synergistic anti-tumor effects of doxorubicin and p53 via graphene oxide-polyethyleneimine nanocarriers. *J Mater Sci Technol*. 2017;33(8):807–814.
37. Dissanayake NM, Current KM, Obare SO. Mutagenic effects of Iron oxide nanoparticles on biological cells. *Int J Mol Sci*. 2015;16(10):23482–23516.
38. Hu C-S, Tang S-L, Chiang C-H, Hosseinkhani H, Hong P-D, Yeh M-K. Characterization and anti-tumor effects of chondroitin sulfate–chitosan nanoparticles delivery system. *J Nanopart Res*. 2014;16(11):1–15.
39. Akhavan O, Ghaderi E. Toxicity of graphene and graphene oxide nanowalls against bacteria. *ACS Nano*. 2010;4(10):5731–5736.
40. Baniasadi H, Ramazani SA, Mashayekhan S, Ramezani Farani M, Ghaderinezhad F, Dabaghi M. Design, Fabrication, and Characterization of Novel Porous Conductive Scaffolds for Nerve Tissue Engineering. *International Journal of Polymeric Materials and Polymeric Biomaterials*. 2015;64(18):969–977.
41. Liu S, Zeng TH, Hofmann M, et al. Antibacterial activity of graphite, graphite oxide, graphene oxide, and reduced graphene oxide: membrane and oxidative stress. *ACS Nano*. 2011;5(9):6971–6980.
42. Vila M, Portolés MT, Marques PA, et al. Cell uptake survey of pegylated nanographene oxide. *Nanotechnology*. 2012;23(46):465103.
43. Shah T. Bioconjugates: The adaptable challenge. *BioPharm Int*. 2013;26(1):34–38.
44. Krishnamoorthy K, Umasuthan N, Mohan R, Lee J, Kim S. Investigation of the antibacterial activity of graphene oxide nanosheets. *Science of Advanced Materials*. 2012;4:1–7.